Supporting Information

An Ultra-Thin Cobalt-Oxide Overlayer Promotes Catalytic Activity of Cobalt Nitride for Oxygen Reduction Reaction

Hadi Abroshan,[†] Pallavi Bothra,[†] Seoin Back, [†] Ambarish Kulkarni,[†] Jens K. Nørskov,[‡,†] and Samira Siahrostami[†] *

[†]SUNCAT Center for Interface Science and Catalysis, Department of Chemical Engineering, Stanford University, 443 Via Ortega, Stanford, California 94305, USA

[‡]SUNCAT Center for Interface Science and Catalysis, SLAC National Accelerator Laboratory, 2575 Sand Hill Road, Menlo Park, California 94305, USA

Corresponding Author

*E-mail: samiras@stanford.edu.

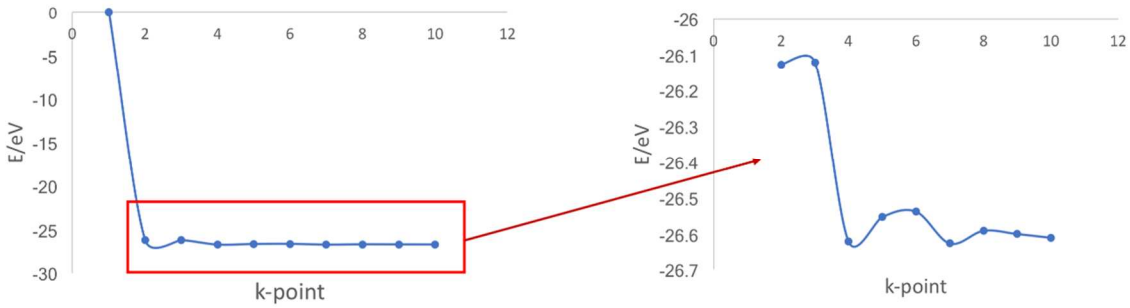

Figure S1. Energy of CoN unit cell as a function of k-point sampling. Energies are reported relative to 1 × 1 × 1 k-point sampling. These results show the use of 8 × 8 × 8 k-point sampling is sufficient.

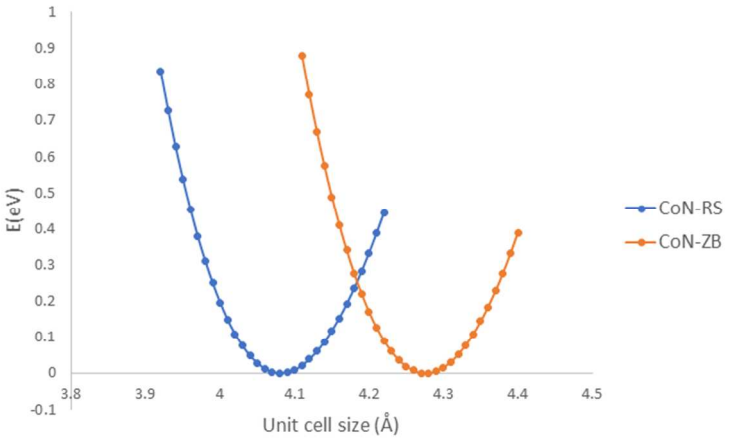

Figure S2. Energy of CoN unit cell in the forms of Rocksalt (RS) and zincblend (ZB) with different sizes. Energies are reported relative to the optimized CoNs. Results demonstrate that the slabs are prepared with minimal strain.

Table S1. To minimize the size dependent error in calculations we examined the calculated limiting potential for several slabs with different numbers of layers. For example, the results for CoN_{RS}(100) with 4-, 6-, and 8-layers are given in Table below. These results show that even systems with 6-layers are sufficient. We have considered 8-layers in all of our calculations. It is worth mentioning, we considered different modes of adsorption, and the systems with lowest energies are taken for calculation of limiting potential.

	4 Layers	6 Layers	8 Layers
CoN_{RS} (100)	0.19	0.14	0.14
CoO/CoN_{RS} (100)	0.67	0.88	0.88

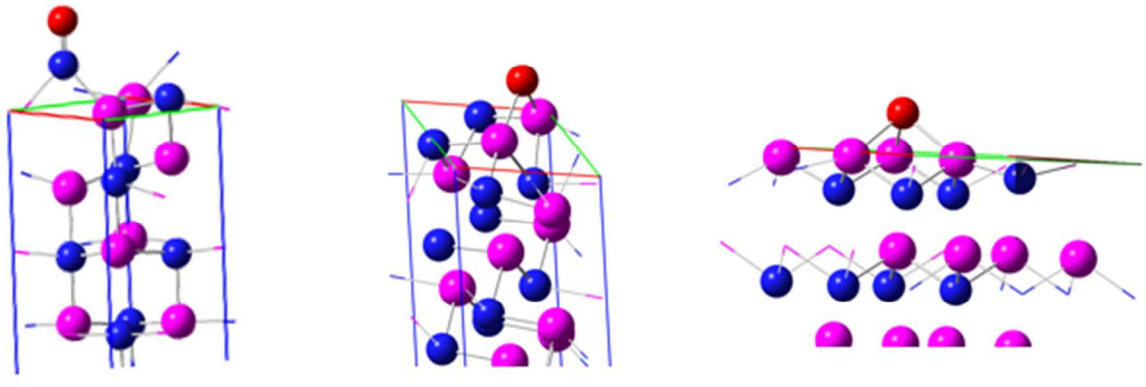

CoN_{RS}(100) CoN_{RS}(110) CoN_{RS}(111)

Figure S3. Optimized structures of adsorbed O* intermediate on different low index facets of the CoN_{RS}; (100), (110), and (111). Color code: Co, pink; N, blue; O, red. Lower part of the slabs are not shown for clarity.

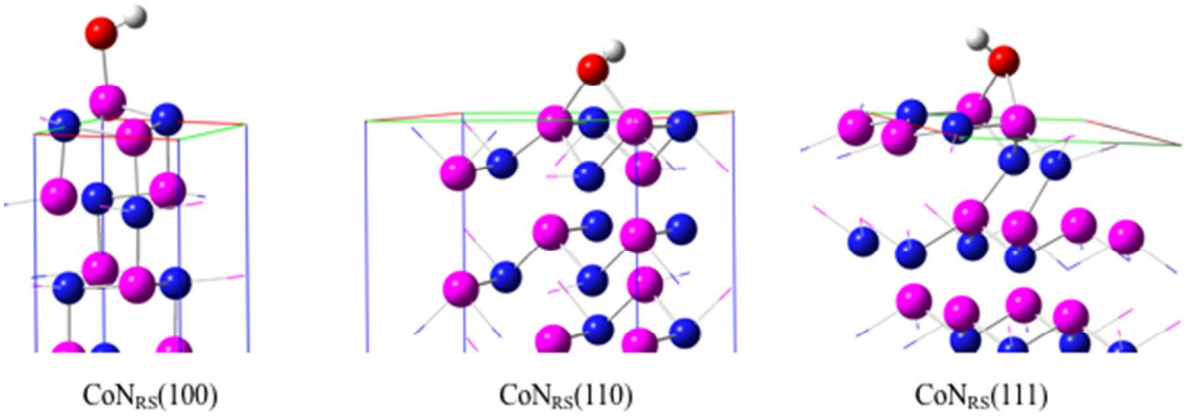

Figure S4. Optimized structure of the adsorbed OH* intermediate on different low index facets of CoN_{RS}; (100), (110), and (111). Color code: Co, pink; N, blue; O, red. Lower part of the slabs are not shown for clarity.

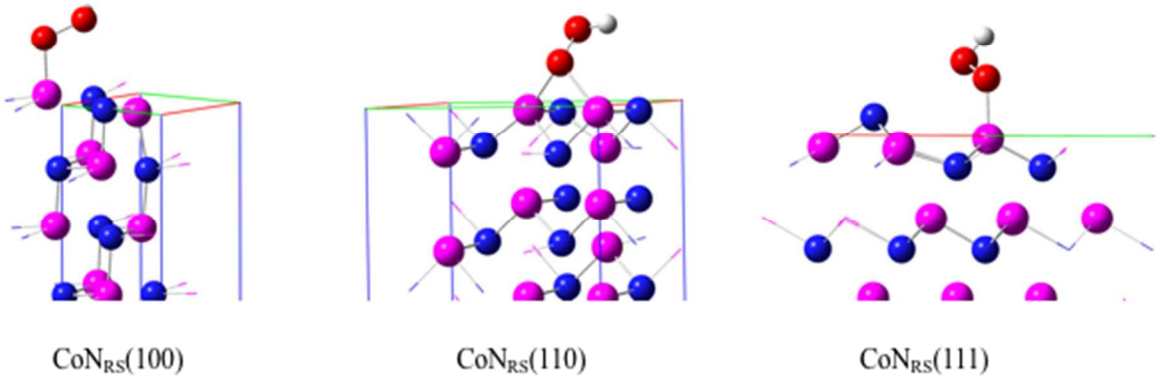

Figure S5. Optimized structure of the adsorbed OOH* intermediate on different low index facets of CoN_{RS}; (100), (110), and (111). Color code: Co, pink; N, blue; O, red. Lower part of the slabs are not shown for clarity.

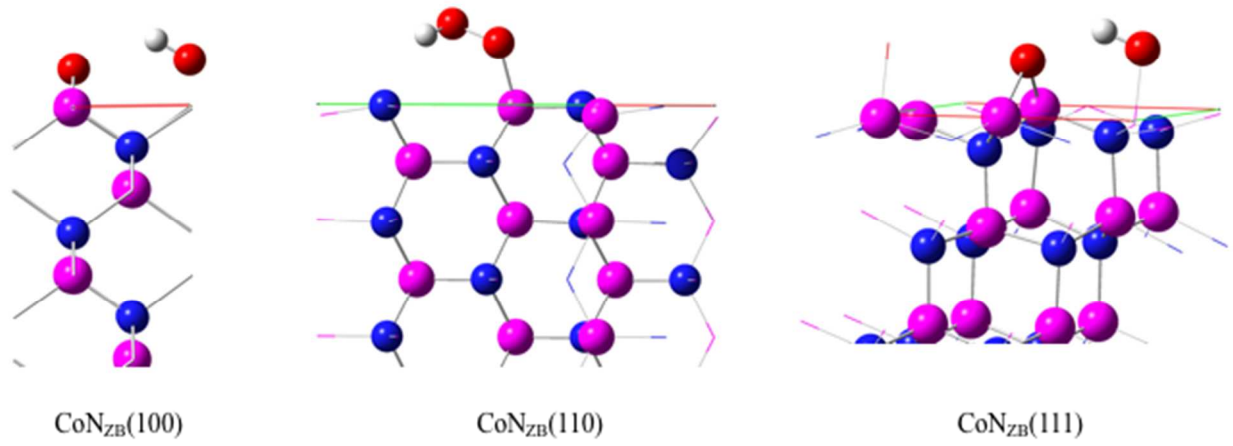

Figure S6. Optimized structure of the adsorbed OOH* intermediate on different low index facets of CoN_{ZB}; (100), (110), and (111). Color code: Co, pink; N, blue; O, red. Lower part of the slabs are not shown for clarity.

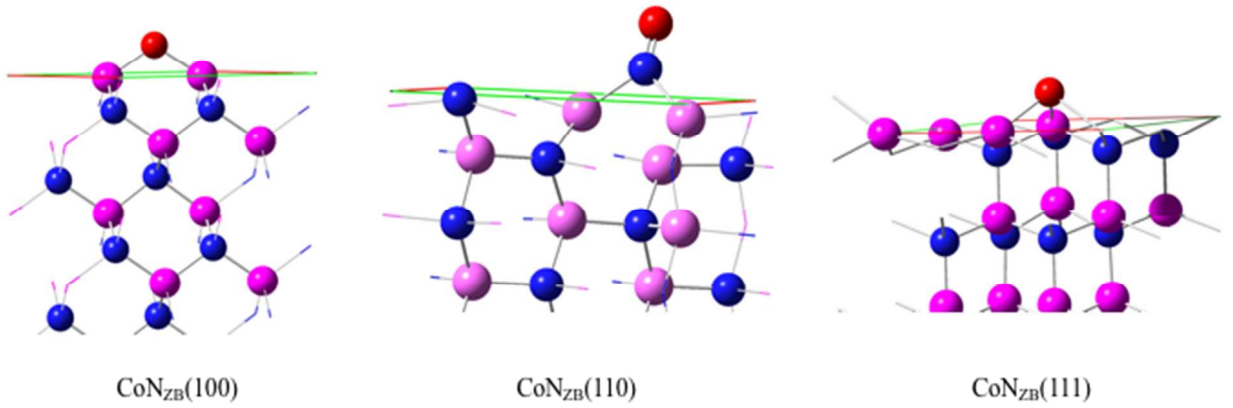

Figure S7. Optimized structure of the adsorbed O* intermediate on different low index facets of CoN_{ZB}; (100), (110), and (111). Color code: Co, pink; N, blue; O, red. Lower part of the slabs are not shown for clarity.

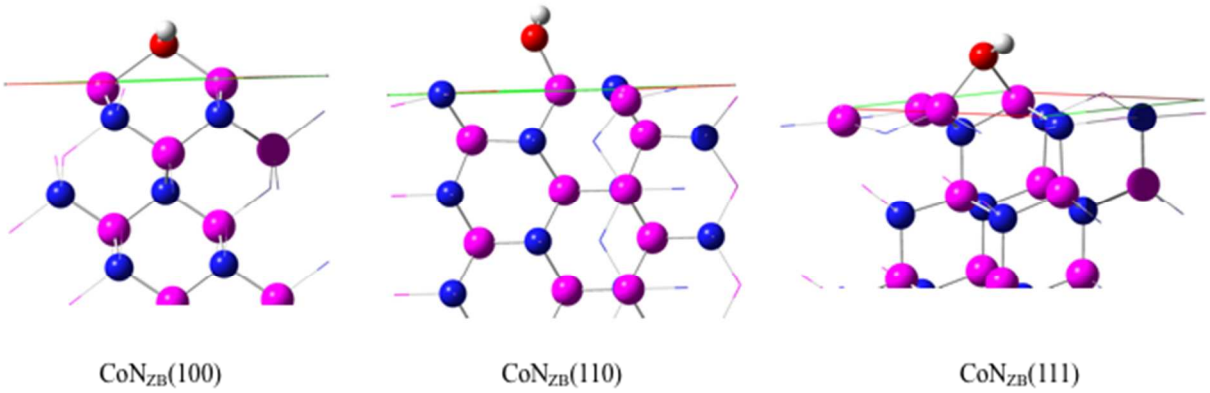

Figure S8. Optimized structure of the adsorbed OH* intermediate on different low index facets of CoN$_{ZB}$; (100), (110), and (111). Color code: Co, pink; N, blue; O, red. Lower part of the slabs are not shown for clarity.

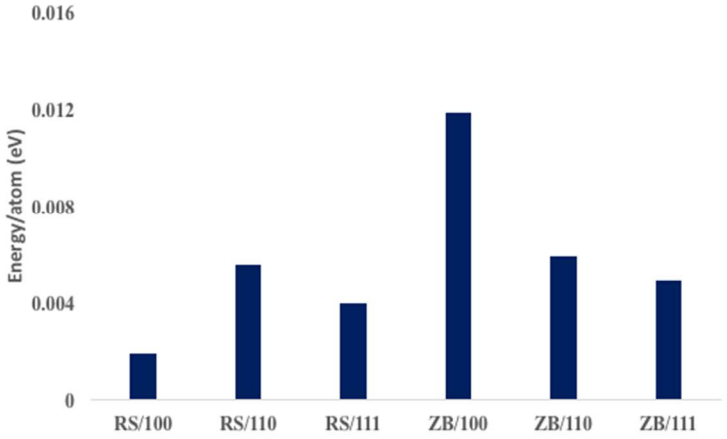

Figure S9. Calculated energy per atom of the slabs in different phases (rocksalt (RS) and zincblend (ZB)) and facets ((100), (110), and (111)) of CoN with respect to the corresponding bulk. .

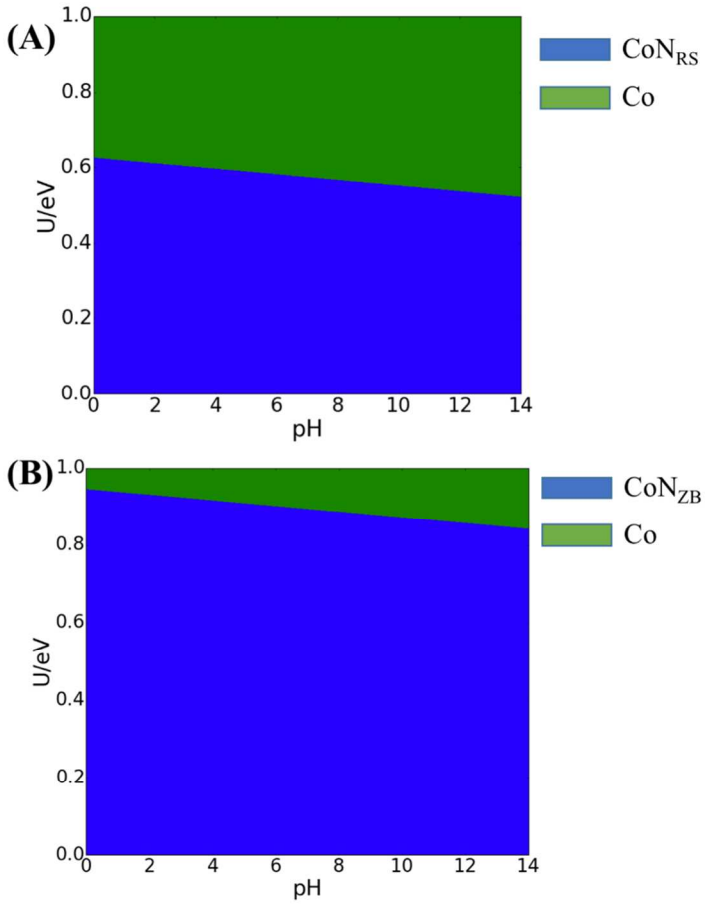

Figure S10. Pourbiax diagrams for the metallic and nitrides of Co as a function of pH and potential (vs HSE) for (A) rocksalt and (B) zincblend phases.

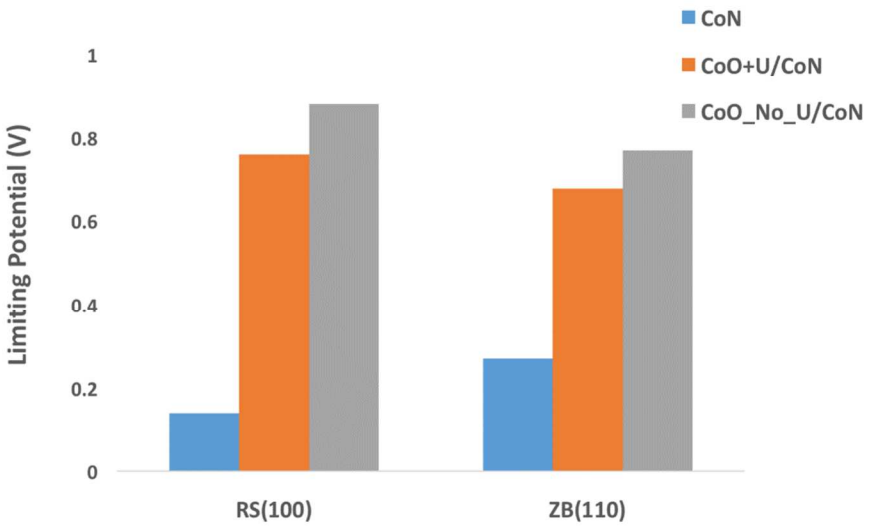

Figure S11. Calculated ORR limiting potentials for $CoN_{RS}(100)$ and $CoN_{ZB}(110)$ in the presence and absence of an oxy-overlayer treated by either DFT or DFT+U.

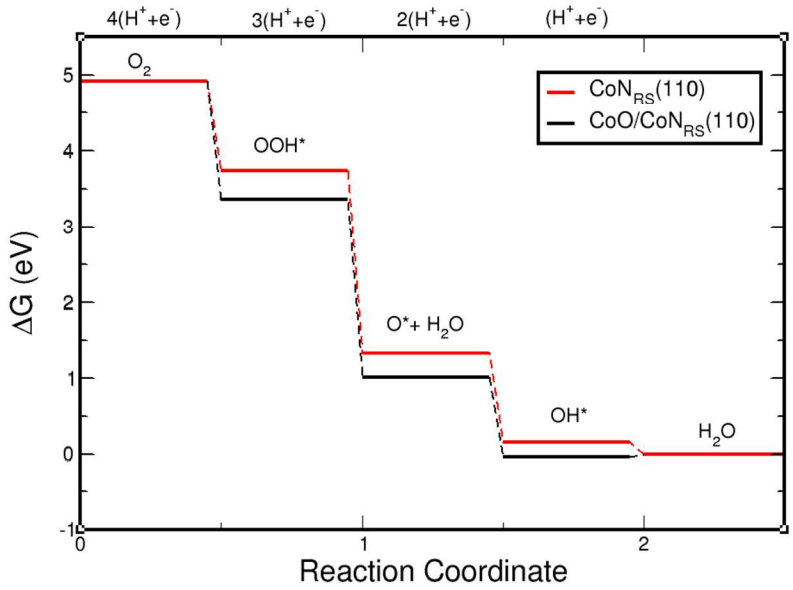

Figure S12. Free energy diagram for oxygen reduction reaction on the facet of $CoN_{RS}(110)$ in the presence and absence of a CoO overlayer at U_{elec} = 0.0 V.

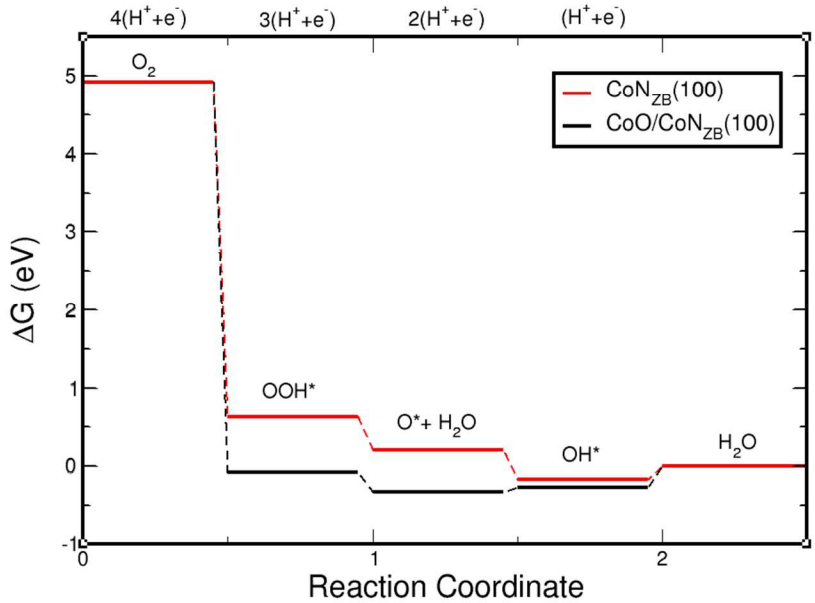

Figure S13. Free energy diagram for ORR on the facet of $CoN_{ZB}(100)$ in the presence and absence of a CoO overlayer at U_{elec} = 0.0 V.

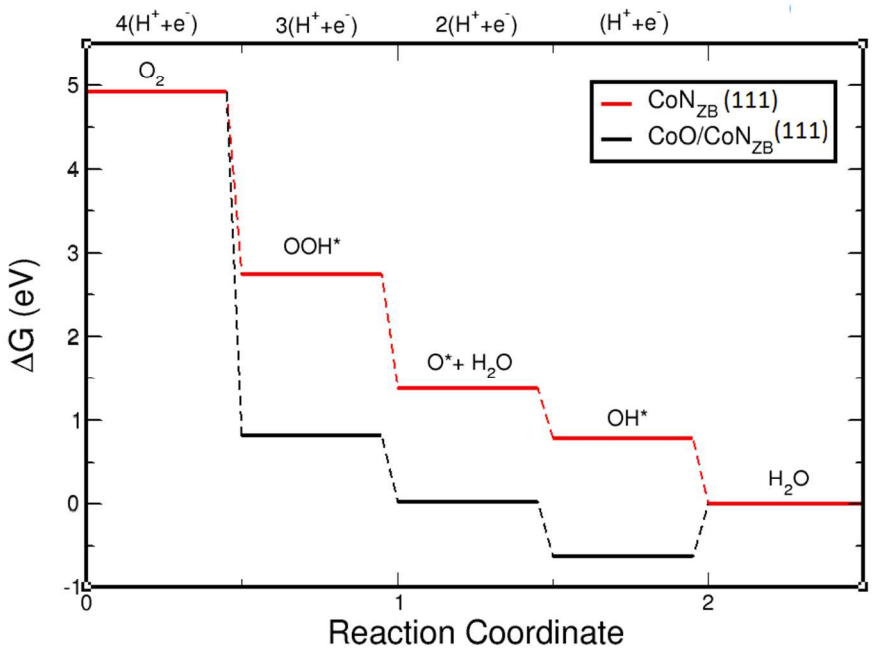

Figure S14. Free energy diagram for ORR on the facet of $CoN_{ZB}(111)$ in the presence and absence of a CoO overlayer at U_{elec} = 0.0 V.

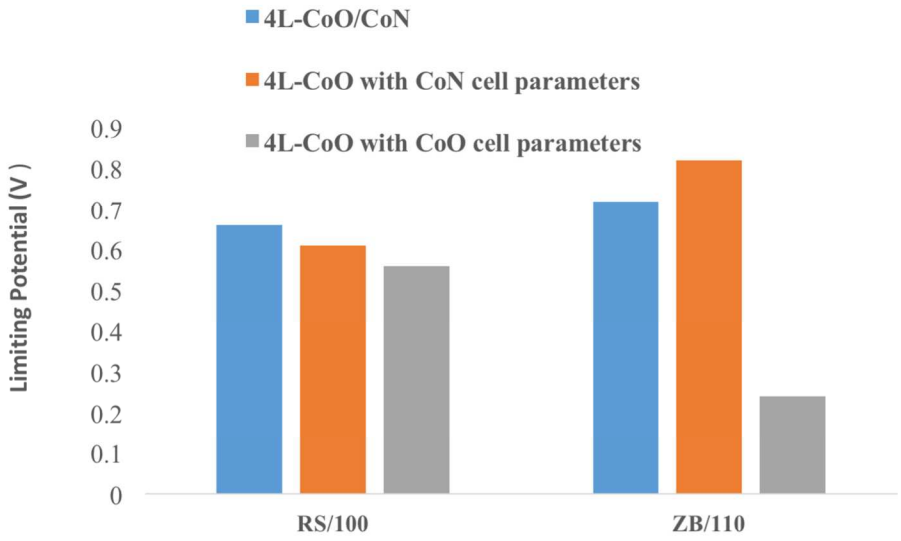

Figure S15. Effects of strain induced by the CoN cell parameters on the ORR limiting potential. The strain has a considerable effect on the limiting potential of CoO in the form of zincblend.

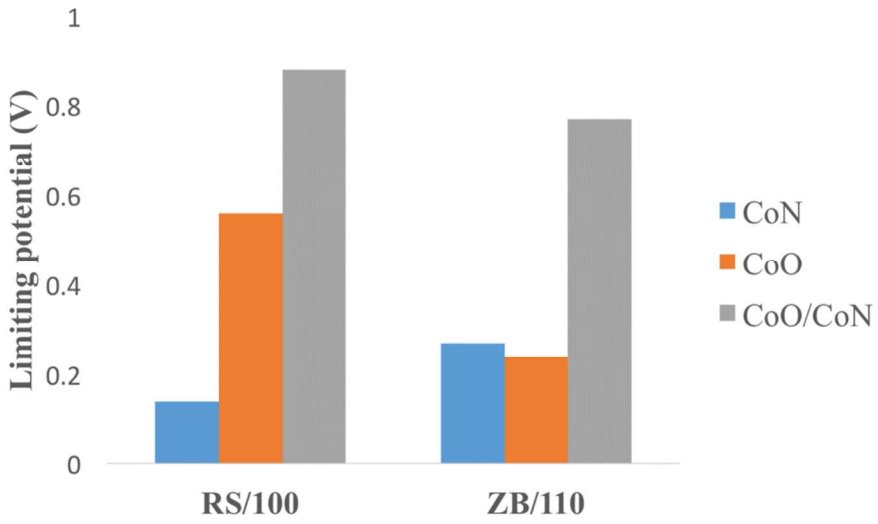

Figure S16. Comparison of the ORR limiting potential over CoN, CoO/CoN, and CoO. Of note, CoO/CoN represents the systems with one oxy-overlayer on the CoNs.